submitted to Proc. of 8th Int. Conf. on Vibrations at Surfaces

Anomalies in He atom scattering spectra of the H-covered Mo (110) and W (110) surfaces

Bernd Kohler, Paolo Ruggerone, and Matthias Scheffler
Fritz-Haber-Institut der Max-Planck-Gesellschaft,
Faradayweg 4-6, D-14 195 Berlin-Dahlem, Germany

(May 1, 1996)

arXiv:mtrl-th/9605002v1 8 May 1996

Helium atom scattering (HAS) studies of the H-covered Mo (110) and W (110) surfaces reveal a twofold anomaly in the respective dispersion curves. In order to explain this unusual behavior we performed density-functional theory calculations of the atomic and electronic structure, the vibrational properties, and the electronic susceptibility of those surfaces. Our work provides evidence for hydrogen adsorption induced Fermi-surface nesting. The respective nesting vectors are in excellent agreement with the HAS data and recent angle resolved photoemission experiments of the H-covered alloy system $Mo_{0.95}Re_{0.05}$ (110). Also, we investigated the electron-phonon coupling and discovered that the Rayleigh phonon frequency is lowered for those critical wave vectors compared to the clean surfaces. Moreover, the smaller indentation in the HAS spectra can be clearly identified as a Kohn anomaly. Based on our results for the susceptibility and the recently improved understanding of the He scattering mechanism we argue that the larger anomalous dip is due to electron-hole excitations by the He scattering.

I. INTRODUCTION

Much interest and many questions have been raised by the recent discovery of deep and extremely sharp indentations in the surface phonon spectra of H/Mo (110) and H/W (110) at full hydrogen coverage [1,2] (see Fig. 1). Those anomalies are seen at an incommensurate wavevector, $\overline{Q}^{c,1}$, along the [001] direction ($\overline{\Gamma H}$) and additionally at the commensurate wavevector $\overline{Q}^{c,2} = \overline{S}$ at the boundary of the surface Brillouin zone (SBZ). Out of the ordinary Rayleigh mode two simultaneous anomalies develop at those points. One, ω_1, is extremely deep, and is only seen by helium atom scattering (HAS). The other, ω_2, is instead soft, and is observed by both HAS and high resolution electron energy loss spectroscopy (HREELS) [3,4].

A pronounced but less sharp softening of surface phonons is also seen on the clean (001) surfaces of W [5] and Mo [6]. There, the effect can be explained in terms of a nested structure of the Fermi surface [7,8]. However, for the phonon anomalies of H/W (110) and H/Mo (110) such a connection between the electronic structure and the vibrational properties seemed to be non-existent since angular resolved photoemission (ARP) experiments of the two systems gave no evidence for nesting vectors comparable to the HAS determined critical wave vectors [9,10]. An alternative model which links the phonon anomalies to the motion of the hydrogen adatoms [3] has to be ruled out because the HAS spectra remain practically unchanged when deuterium is adsorbed instead of hydrogen [1,2].

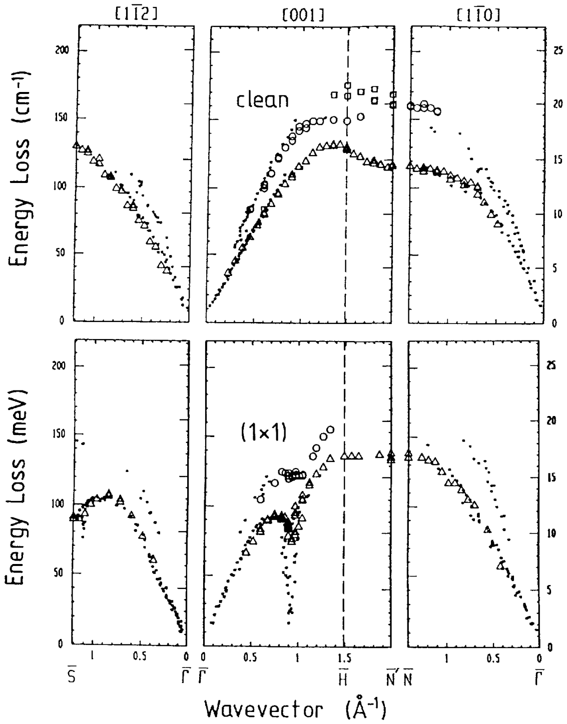

FIG. 1. HREELS spectra of the clean W(110) surface (upper panel) and its H-covered (1 × 1) phase (lower panel) [3,4]: Shown are the dispersion of the Rayleigh wave (triangles) and the longitudinally polarized surface phonons of the first (circles) and second (squares) layer. The dots represent the results of the HAS measurements [1,2].

Another puzzle is added by the observation of a symmetry loss in the low-energy electron diffraction (LEED) pattern of W (110) upon H-adsorption. The phenomena may be caused by a H-induced displacement of the top layer W atoms along the [$\overline{1}$10] direction [11] (see Figs. 2b and c). Similar studies for H/Mo (110) do not provide any evidence for a top-layer-shift reconstruction [12].

Within a first-principles approach, the goal of our work is to give a comprehensive explanation for the observed anomalous behavior and clarify the confusing picture drawn by the different experimental findings.

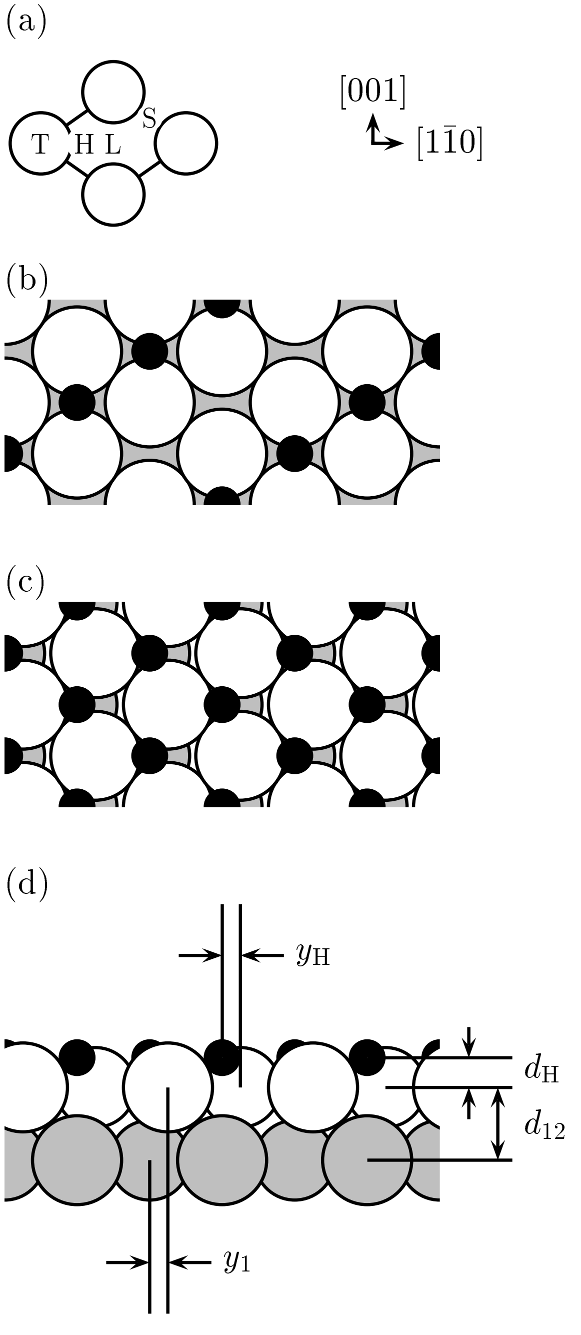

FIG. 2. (a) Adsorbate positions within the $p(1 \times 1)$ unit cell of the W (110) and Mo (110) surfaces: Shown are the long-bridge (L), short-bridge (S), hollow (H), and on-top (T) site. (b-c) Structure of the H-covered W (110) surface as suggested by Chung *et al.* [11]: (b) low H-coverage $\Theta < 0.5$ ML; (c) top-layer-shift reconstruction for higher H-coverages $\Theta > 0.5$ ML. The white (shaded) circles represent the W/Mo atoms of the surface (subsurface) layer. The H positions are indicated by full dots. (d) Structure parameters used in Table I.

II. METHOD

We perform density-functional theory (DFT) calculations using the local-density approximation (LDA) for the exchange-correlation energy functional [13]. For the self-consistent solution of the Kohn-Sham equations a full-potential linearized augmented plane-wave (FP-LAPW) code [14] is employed which we enhanced by the direct calculation of atomic forces [15,16]. Within a damped molecular dynamics approach this enables an efficient determination of fully relaxed atomic geometries and frozen-phonon energies. For methodical details we refer to Ref [17]. In the case of the W surfaces the valence and semi-core (core) electrons are treated scalar (fully) relativistically while for Mo all electrons are handled non-relativistically. The in-plane lattice constants $a_\mathrm{W}^\mathrm{theo} = 3.14$ Å and $a_\mathrm{Mo}^\mathrm{theo} = 3.13$ Å are calculated without including zero-point vibrations. They are in good agreement with the respective measured bulk lattice parameters at room temperature which are 3.163 Å and 3.148 Å for W [18] and Mo [19], respectively.

We performed systematic tests comparing the LDA and the generalized gradient approximation [20] exchange-correlation functionals. For the quantities reported in this paper (total energy differences of different adsorption sites, bond lengths, etc.) both treatments give practically the same results. Also, we checked the $\mathbf{k}_\parallel$-point convergence: In the case of atomic and electronic structure calculations a two-dimensional linear mesh of 64 $\mathbf{k}_\parallel$-points within the (1×1) SBZ gives stable results. For the evaluation of frozen-phonon energies a set of 56 $\mathbf{k}_\parallel$-points is employed within the SBZ of the enlarged (1×2) and (2×1) surface cells.

III. RESULTS

A. Atomic Structure

The first step in our study is to determine the atomic structures of the clean and hydrogen-covered (110) surfaces. The relaxation parameters presented in Table I are calculated for a nine-layer slab (the parameters are defined in Fig. 2d). The results, which are remarkably similar for Mo and W, are in excellent quantitative agreement with a recent LEED analysis [21,22].

As the energetically most favorable hydrogen adsorption site on both W (110) and Mo (110) we identify a quasi-threefold position (indicated as H in Fig. 2a). Our investigations also throw light on the suggested model of a H-induced structural change: For both materials the calculated shift y_1 is only of the order of 0.01 Å and thus there is no evidence for a pronounced top-layer-shift reconstruction. Moreover, this subtle change in the surface

TABLE I. Relaxation parameters for the clean and H-covered (110) surfaces of Mo and W (see also Fig. 2d). For each system the results from a nine-layer slab calculation (first line) and a LEED analysis (second line) [21,22] are presented. The height of the hydrogen above the surface and its $[\bar{1}10]$ offset from the [001] bridge position are denoted by d_{H} and y_{H}, respectively. The shift of the surface layer with respect to the substrate is y_1. The parameters Δd_{ij} describe the percentage change of the interlayer distance between the i-th and the j-th substrate layers with respect to the bulk interlayer spacing d_0. The numerical accuracy of the theoretically obtained parameters is ± 0.015 Å$\approx \pm 0.7\% d_0$.

y_{H} (Å)	d_{H} (Å)	y_1 (Å)	Δd_{12} ($\% d_0$)	Δd_{23} ($\% d_0$)	Δd_{34} ($\% d_0$)
			Mo (110)		
–	–	–	-5.0	$+0.7$	-0.3
–	–	–	-4.0 ± 0.6	$+0.2 \pm 0.8$	0.0 ± 1.1
			H/Mo (110)		
0.62	1.09	0.04	-3.3	$+0.3$	-0.2
0.55 ± 0.4	1.3 ± 0.3	0.0 ± 0.1	-2.0 ± 0.4	0.0 ± 0.5	0.0 ± 0.8
			W (110)		
–	–	–	-3.6	$+0.2$	-0.3
–	–	–	-3.1 ± 0.6	0.0 ± 0.9	0.0 ± 1.0
			H/W (110)		
0.67	1.09	0.02	-1.4	-0.3	-0.1
0.56 ± 0.4	1.2 ± 0.25	0.0 ± 0.1	-1.7 ± 0.5	0.0 ± 0.6	0.0 ± 0.9

geometry is unlikely to be resolved experimentally due to zero-point vibrations. This aspect becomes evident by evaluating the total energy with respect to a rigid top-layer-shift. In Fig. 3 we present the results of such a calculation for H/W (110) and depict the first three vibrational eigenstates obtained from a harmonic expansion of the total energy $E^{\mathrm{tot}}(y_1)$; for H/Mo (110) the energetics is similar. Since we have $k_{\mathrm{B}}T \approx 25$ meV at room temperature thermal fluctuations of y_1 are of the order of 0.1 Å. This is considerably larger than the theoretically predicted absolute value of y_1.

B. Electronic Structure

The similarities between Mo (110) and W (110) found for the surface geometries continue when we compare the electronic structures. For both systems the H adsorption alters the surface potential and induces the shift of a band with $(d_{3z^2-r^2}, d_{xz})$ character to higher binding energies [17,23]. Due to this effect which is illustrated in Fig. 4 the Fermi line associated with this band is moved into the band gap of the surface projected band structure, and the respective states become true surface states.

The shifted $(d_{3z^2-r^2}, d_{xz})$ band is characterized by a

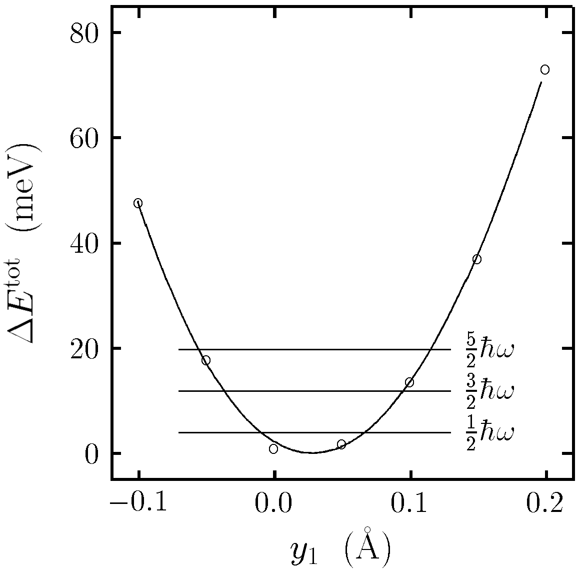

FIG. 3. Change of total energy E^{tot} versus top-layer-shift y_1: For each data point the whole surface is relaxed keeping only the substrate $[1\bar{1}0]$-coordinates y_1 and $y_2 = y_3 = 0$ Å fixed. Also shown are the first three oscillator eigenstates calculated from a harmonic expansion of the total energy $E^{\mathrm{tot}}(y_1)$.

high density of states at the Fermi level. More important, the new Fermi contour shows pronounced nesting features (see Fig. 5c). The magnitudes of the calculated nesting vectors and HAS measured critical wavevectors along $\overline{\Gamma S}$ and $\overline{\Gamma H}$ are listed in Table II. For both systems the agreement between theory and experiment is excellent.

Our results are at variance with the photoemission studies by Kevan and coworkers [9,10] (see Fig. 2 in Ref. [17]). However, in view of more recent ARP measurements [24] which we compare to our results in Fig. 5 we dare to suggest that those differences may be due to problems in the experimental analysis. The later work deals with the (110) surface of the alloy $\mathrm{Mo}_{0.95}\mathrm{Re}_{0.05}$ but the surface physics of both systems $\mathrm{Mo}_{0.95}\mathrm{Re}_{0.05}$ (110) and Mo (110) should be practically the same because in

TABLE II. Theoretical Fermi-surface nesting vectors compared to critical wavevectors obtained by HAS and HREELS experiments [1,2,3].

direction	system	$\lvert\overline{Q}^{\mathrm{c}}\rvert$ (Å^{-1}) theory	experiment
$\overline{\Gamma H}$	H/Mo (110)	0.86	0.90
	H/W (110)	0.96	0.95
$\overline{\Gamma S}$	H/Mo (110)	1.23	1.22
	H/W (110)	1.22	1.22

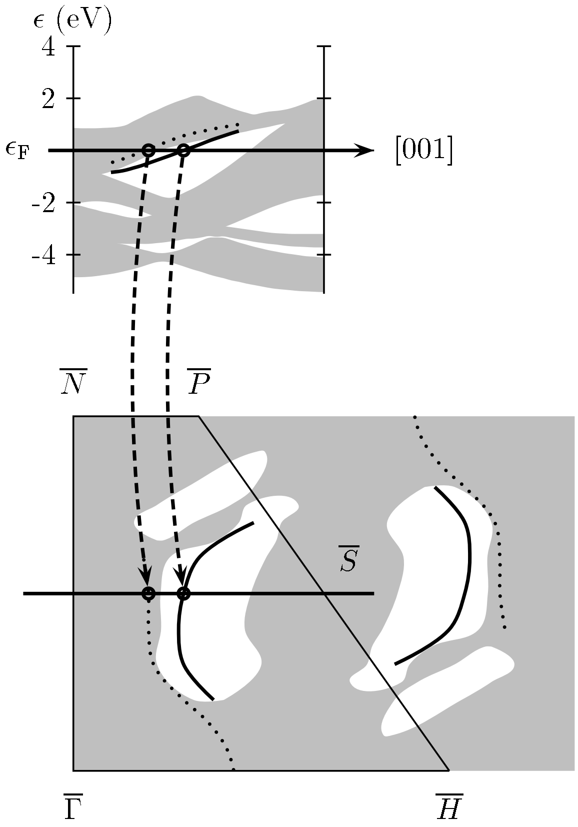

FIG. 4. Band structure (upper figure) and Fermi surface (lower figure) of clean Mo (110) (dotted curves) and H/Mo (110) (solid curves). The shaded areas represent the projection of the bulk Fermi surface onto the SBZ of the (110) surface.

both cases the top layer consists only of Mo atoms. This assumption is also backed by test calculations where we simulated a $Mo_{0.95}Tc_{0.05}$ alloy be the virtual crystal approximation and found only minor quantitative changes.

From Fig. 5 it becomes clear that in particular for the important $(d_{3z^2-r^2}, d_{xz})$ surface band, which was not seen by Kevan's group, experiment and DFT now agree very well. There are however differences: Theory predicts bands centered at $\overline{S}$ which are not seen by ARP whereas the band circle at $\overline{\Gamma}$ in Fig. 5d is only observed experimentally. Also, in the calculations we find an elliptical band centered at the $\overline{\Gamma}$ point whereas in ARP the same band has the shape of a rectangle. Those discrepancies are probably due to the fact that it is rather difficult in theory (and experiment!) to clearly distinguish between surface states and surface resonances. Additionally, due to interactions between the two surfaces within a slab system the $\mathbf{k}_{\parallel}$-space location of a calculated surface resonance which is not strongly localized at the surface cannot be determined accurately. Furthermore, we note that DFT is not expected to describe the Fermi surface accurately. Nevertheless, the important theoretical finding of a H-induced surface state which can be related to the HAS anomalies is now verified by experiment.

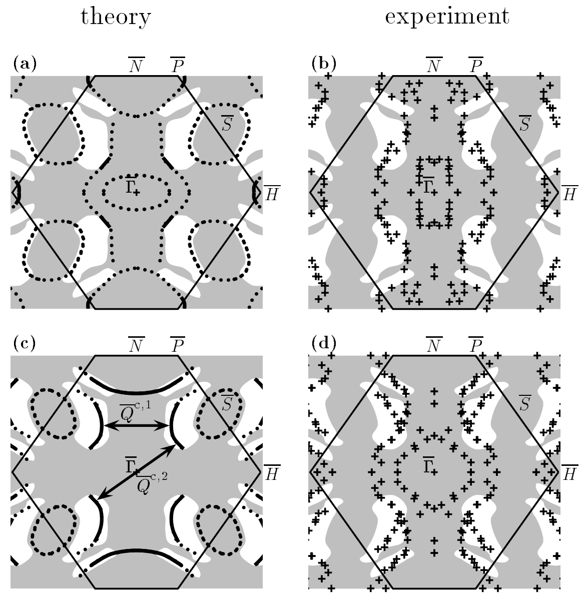

FIG. 5. Theoretical Fermi surfaces of the (a) clean and (c) H-covered Mo (110) surface. The solid (dotted) lines denote surface resonances or surface states which are localized by more than 60 % (30 %) in the MTs of the two top Mo layers. Shaded areas represent the (110) projected theoretical Mo bulk Fermi surface. The arrows $\overline{Q}^{c,1}$ and $\overline{Q}^{c,2}$ are the critical wave vectors predicted by the calculations. Also presented are data points (+) which stem from an ARP study of the (b) clean and (d) H-covered $Mo_{0.95}Re_{0.05}$ (110) surface [24].

C. Vibrational Properties

At this point, the following question arises: How does the surface react to the apparent electronic instability due to the strong nesting features? In the case of nesting the surface phonons take the burden to furnish energy and momentum to the scattering process of electrons at the Fermi level. This leads to a softening of the related phonons. If the electron-phonon coupling is strong and the energetic cost of a surface distortion is small this softening could even trigger a reconstruction combined with the build-up of a charge-density wave as in the case of the (001) surfaces of W [5] and Mo [6]. It is clear that one needs to perform frozen-phonon calculations in order to determine the actual strength of the coupling and the induced phonon softening [25].

Fortunately, at $\overline{Q}^{c,2} = \overline{S}$ such a calculation is particularly convenient, since at the zone boundary point $\overline{S}$ the Rayleigh-wave polarization is purely vertical, and the second layer is immobile by symmetry. The calculated frequencies for the $\overline{S}$-point and a second zone boundary point, $\overline{N}$, are presented in Table III. For the latter our

TABLE III. Comparison of calculated frozen-phonon energies and experimental values obtained by HAS [1,2] and HREELS [3]. The theoretical phonon energies are obtained using a five-layer slab. Their numerical accuracy is about ±1 meV.

phonon	system	E^{ph} (meV)	
		theory	experiment
$\overline{N}$	W (110)	15.4	14.5
	H/W (110)	17.6	17.0
$\overline{S}$	Mo (110)	22.7	∼21
	H/Mo (110)	17.2	<16
	W (110)	18.3	16.1
	H/W (110)	12.0	11.0

results reproduce the experimentally observed increase of the Rayleigh wave frequency as hydrogen is adsorbed. At the $\overline{S}$ point we find that those stiffening effects are overcompensated: The strong coupling to electronic states at the Fermi level leads to a lowering of the phonon energy in good agreement with the experimental results.

In Fig. 6 we schematically illustrate the mechanism which is responsible for this effect. It is, in fact, a textbook example of a Kohn anomaly due to Fermi-surface nesting [26,27]: (a) Within the unperturbated system the $(d_{3z^2-r^2}, d_{xz})$ band cuts the Fermi level exactly midway between $\overline{\Gamma}$ and $\overline{S}$. (b) The $\overline{S}$-point phonon couples to the states at the Fermi level and causes the backfolding of the SBZ. (c) The nuclear distortion associated with the $\overline{S}$-point phonon modifies the surface potential and hence removes the degeneracy at the new zone boundary point $\overline{S'}$. The occupied states are shifted to lower energies. This amounts to a negative contribution of the electronic band structure energy to the total energy and thus a lowering of the phonon energy.

A frozen-phonon study for the second nesting vector along $\overline{\Gamma H}$ is not performed because $\overline{Q}^{\mathrm{c},1}$ is highly noncommensurate; a calculation would be very expensive. However, since the character of the $(d_{3z^2-r^2}, d_{xz})$ band does not change when shifting from the $\overline{\Gamma S}$ to the $\overline{\Gamma H}$ nesting we expect similar results.

The calculation of the electron-phonon interaction at the Mo (110) and W (110) surfaces and its change due to hydrogen adsorption pinpoints the phonon character of the small anomaly ω_2 and identifies the interplay between the electronic structure and the vibrational spectra of the transition metal surfaces. Thus, our results which were recently confirmed by Bungaro [28] within the framework of perturbation DFT clearly support the interpretation that the small dip observed by both HAS and HREELS is due to a Kohn anomaly.

(a) original Brillouin zone

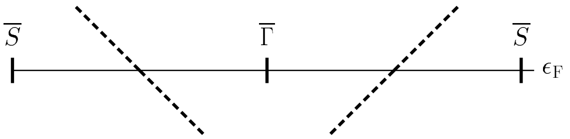

(b) backfolding ($\overline{\Gamma S'} = \frac{1}{2}\overline{\Gamma S}$)

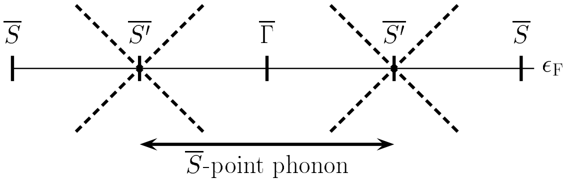

(c) phonon

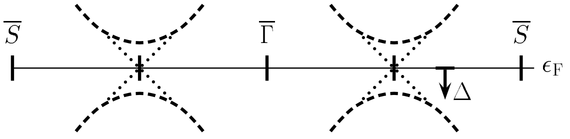

FIG. 6. Schematic representation of the mechanism which causes the Kohn anomaly on H/Mo (110) and H/W (110). Shown is the bandstructure along $\overline{S\Gamma S}$ parallel to the nesting vector $\overline{Q}^{\mathrm{c},2}$ in Figs. 5. The form of the $(d_{3z^2-r^2}, d_{xz})$ band is indicated by dashed lines.

D. Electron-hole excitations

For the deep and sharp anomaly ω_1 the interpretation is less straightforward, particularly since it is only seen in the HAS spectra. One needs to understand the nature of rare-gas scattering in order to explain this unusual behavior.

In a recent study we found that those scattering processes are significantly more complicated (and more interesting) than hitherto assumed [29]: The reflection of the He atom happens in front of the surface at a distance of 2–3 Å. More important, it is not the *total* electron density of the substrate surface which determines the interaction but the electronic wave functions close to the Fermi level. In the case of the H/W (110) and H/Mo (110) systems it is thus plausible to assume that the He atom couples directly to the $(d_{3z^2-r^2}, d_{xz})$ surface states mentioned above and excites electron-hole pairs.

In order to analyze the spectrum of those excitations in some more detail we evaluate the imaginary part of the electronic susceptibility $\chi(\mathbf{q}_{\|}, \hbar\omega)$ within random phase approximation (RPA):

$$\begin{aligned} &\mathrm{Im}\,\chi(\mathbf{q}_{\|}, \hbar\omega) = \\ &= \mathrm{Im}\frac{A}{4\pi^2}\int_{\mathrm{SBZ}} d\mathbf{k}_{\|}\; w_{\mathbf{k}_{\|}+\mathbf{q}_{\|}} w_{\mathbf{k}_{\|}}\; (f_{\mathbf{k}_{\|}+\mathbf{q}_{\|}} - f_{\mathbf{k}_{\|}}) \times \end{aligned}$$

$$
\begin{aligned}
& \times \frac{1}{\varepsilon_{\mathbf{k}_\parallel+\mathbf{q}_\parallel} - \varepsilon_{\mathbf{k}_\parallel} - \hbar\omega - i\eta} \\
= \; & \frac{A}{4\pi^2}\int_{\mathrm{SBZ}} d\mathbf{k}_\parallel \; w_{\mathbf{k}_\parallel+\mathbf{q}_\parallel} w_{\mathbf{k}_\parallel} \; (f_{\mathbf{k}_\parallel+\mathbf{q}_\parallel} - f_{\mathbf{k}_\parallel}) \times \qquad (1) \\
& \times \delta\left(\varepsilon_{\mathbf{k}_\parallel+\mathbf{q}_\parallel} - \varepsilon_{\mathbf{k}_\parallel} - \hbar\omega\right)
\end{aligned}
$$

with $\frac{A}{4\pi^2}$ being the $\mathbf{k}_\parallel$-space density. In our approach we use all eigenvalues $\epsilon_{\mathbf{k}_\parallel}$ and occupation numbers $f_{\mathbf{k}_\parallel}$ obtained via a nine-layer slab calculations. Also, we take into account the localization $w_{\mathbf{k}_\parallel}$ of the respective state at a distance of 2.5 Å in front of the substrate surface.

The results obtained for Mo (110) and H/Mo (110) are presented in Fig. 7: For the clean surface we find that the intensity of the electron-hole excitations decreases continuously as we move away from the $\overline{\Gamma}$ point towards the zone boundaries. This relatively smooth behavior of the susceptibility is modified considerably when H is adsorbed on the clean surface: Pronounced peaks appear, in particular one which stretches from the $\overline{\Gamma H}$ line through the SBZ to the symmetry point $\overline{S}$. This is in excellent agreement with the HAS results. Also, there is a peak located at the second half of the $\overline{\Gamma N}$ symmetry line. It cannot be associated with an anomaly in the HAS spectrum. This result may be due to the fact that selection rules for the interaction between the scattering He atoms and the electron-hole excitations are not considered.

In view of the simplicity of the approach, the calculated spectrum of electron-hole excitations however seems to be well-connected to the HAS measurements. Moreover, it is surprising how detailed the Fermi surface nesting is reflected in the susceptibility at such a large distance from the surface where the HAS scattering process takes place. This finding supports the earlier suggestion [17] that the giant indentations, seen only in HAS, are due to the excitation of electron-hole pairs. By contrast, in HREELS experiments the electrons are directly scattered at the atoms and thus only measure the phonon spectrum. Therefore, the strong anomaly is invisible for HREELS.

IV. SUMMARY

In conclusion, the major results of our work are as follows: We demonstrate that both the W (110) and the Mo (110) surface do not show a pronounced top-layer-shift reconstruction upon adsorption of hydrogen, a result confirmed by a recent LEED analysis [21]. Also, we give a consistent explanation for the H-induced anomalies in the HAS spectra of W (110) and Mo (110). The H adsorption induces surface states of $(d_{3z^2-r^2}, d_{xz})$ character that show pronounced Fermi-surface nesting. The soft anomalous dip is clearly identified as a Kohn anomaly due to those nesting features [17,23,25]. For an understanding of the huge dip one needs to take into account that the scattering of rare-gas atoms is crucially influenced by interactions with substrate surface wave func-

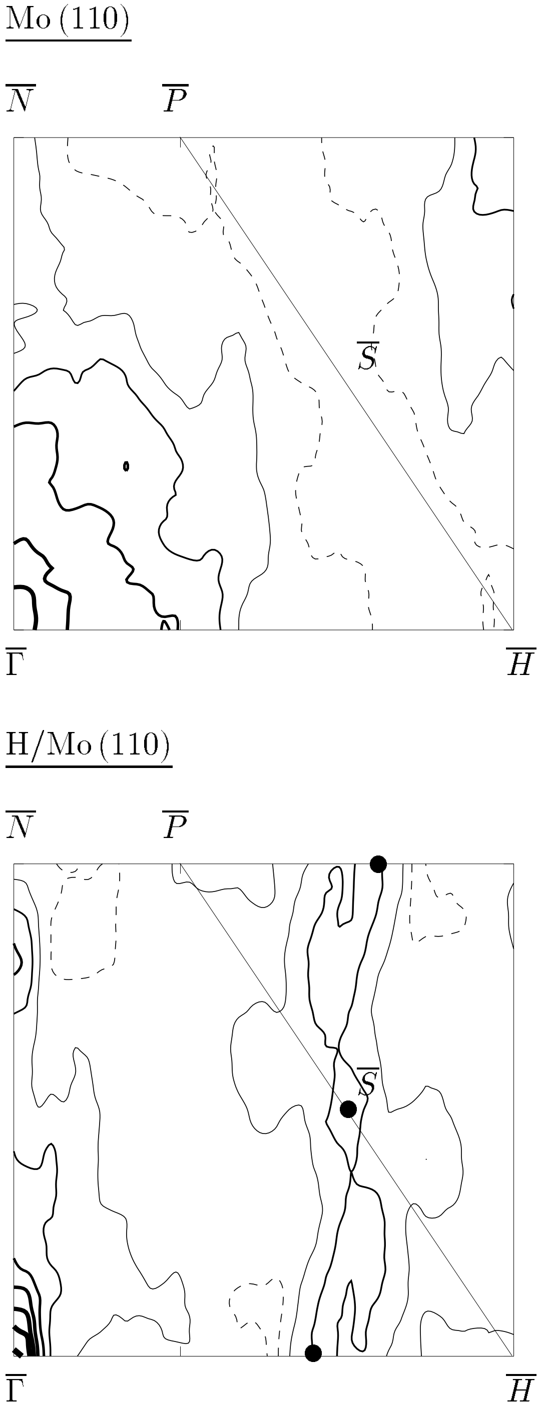

FIG. 7. Imaginary part of the electronic RPA susceptibility $\chi(\mathbf{q}_\parallel, \hbar\omega)$ of Mo (110) and H/Mo (110) calculated for $\hbar\omega = 0.5\,\mathrm{mRy} \approx 7\,\mathrm{meV}$. The dashed line represents a value of 3 a.u. while each full line denotes an additional increase by 1 a.u. (with increasing line width). The positions of the HAS measured anomalies within the SBZ are indicated by dots.

tions at the Fermi level [29]. The He atom couples efficiently to the H-induced surface states on H/W (110) and H/Mo (110). We therefore conclude that the deep branch of the anomaly is predominantly caused by a direct excitation of electron-hole pairs during the scattering process.

We hope that our first-principles study stimulates some more experimental work: For instance, the liquid-like behavior of the H adatoms observed in the HREELS measurements [3] is still not understood. One would also like to know whether the HAS and HREELS spectra of the $\mathrm{Mo}_{0.95}\mathrm{Re}_{0.05}$ (110) alloy system reveal H-induced anomalies as expected. Finally, we call for a new ARP study of the clean and H-covered Mo (110) and W (110) surface and think that scattering experiments with atoms or molecules like Ne or H_2 might provide additional insight into the interesting behavior of these surfaces.

We thank Erio Tosatti for stimulating discussions.

---

[1] E. Hulpke and J. Lüdecke, Phys. Rev. Lett. **68**, 2846 (1992); J. Electron. Spectr. Relat. Phenom. **64/65** (1993) 641.

[2] J. Lüdecke, Ph.D. thesis (Universität Göttingen, 1994).

[3] M. Balden, S. Lehwald, H. Ibach, and D. L. Mills, Phys. Rev. Lett. **73** (1994) 854.

[4] M. Balden, Ph. D. thesis (RWTH Aachen, 1995).

[5] H.-J. Ernst, E. Hulpke, and J. P. Toennies, Phys. Rev. B **46** (1992) 16081.

[6] E. Hulpke and D.-M. Smilgies, Phys. Rev. B **40** (1989) 1338.

[7] K. E. Smith, G. S. Elliott, and S. D. Kevan, Phys. Rev. B **42** (1990) 5385.

[8] J. W. Chung, K. S. Shin, D. H. Baek, C. Y. Kim, H. W. Kim, S. K. Lee, C. Y. Park, S. C. Hong, T. Kinoshita, M. Watanabe, A. Kakizaki, and T. Ishii, Phys. Rev. Lett. **69** (1992) 2228.

[9] K. H. Jeong, R. H. Gaylord, and S. D. Kevan, Phys. Rev. B **38** (1988) 10302; Phys. Rev. B **39** (1989) 2973; J. Vac. Sci. Technol. A **7** (1989) 2199.

[10] R. H. Gaylord, K. H. Jeong, and S. D. Kevan, Phys. Rev. Lett. **62** (1989) 2036.

[11] J. W. Chung, S. C. Ying, and P. J. Estrup, Phys. Rev. Lett. **56** (1986) 749.

[12] M. Altman, J. W. Chung, P. J. Estrup, J. M. Kosterlitz, J. Prybyla, D. Sahu, and S. C. Ying, J. Vac. Sci. Technol. A **5** (1987) 1045.

[13] D. M. Ceperley and B. J. Alder, Phys. Rev. Lett. **45** (1980) 566; J. P. Perdew and A. Zunger, Phys. Rev. B **23** (1981) 5048.

[14] P. Blaha, K. Schwarz, P. Sorantin, and S. B. Trickey, Comput. Phys. Commun. **59** (1990) 399; P. Blaha, K. Schwarz, R. Augustyn, WIEN93 (Technische Universität Wien, 1993).

[15] R. Yu, D. Singh, and H. Krakauer, Phys. Rev. B **43** (1991) 6411.

[16] B. Kohler, S. Wilke, M. Scheffler, R. Kouba, and C. Ambrosch-Draxl, Comput. Phys. Commun. **94** (1996) 31.

[17] B. Kohler, P. Ruggerone, S. Wilke, and M. Scheffler, Phys. Rev. Lett. **74** (1995) 1387.

[18] J. S. Shah and M. E. Straumanis, J. Appl. Phys. **42** (1971) 3288.

[19] K. W. Katahara, M. H. Manghnani, and E. S. Fisher, J. Phys. F **9** (1979) 773.

[20] J. P. Perdew and Y. Wang, Phys. Rev. B **45** (1992) 13244.

[21] M. Arnold, L. Hammer, K. Heinz, B. Kohler, and M. Scheffler, to be published.

[22] M. Arnold, private communication.

[23] P. Ruggerone, B. Kohler, S. Wilke, and M. Scheffler, in: Electronic Surface and Interface States on Metallic Systems, Eds. E. Bertel and M. Donath (World Scientific, Singapore, 1995) p. 113.

[24] M. Okada, A. P. Baddorf, D. M. Zehner, and E. W. Plummer, in press, Surf. Sci. (1996).

[25] B. Kohler, P. Ruggerone, M. Scheffler, and E. Tosatti, to be published in Z. Phys. Chem.

[26] A. B. Migdal, Sov. Phys. JETP **34** (1958) 996.

[27] W. Kohn, Phys. Rev. Lett. **2** (1959) 393.

[28] C. Bungaro, Ph.D. thesis (SISSA, Trieste, 1995).

[29] M. Petersen, S. Wilke, P. Ruggerone, B. Kohler, and M. Scheffler, Phys. Rev. Lett. **76** (1996) 995.